

# Giant adsorption of microswimmers: duality of shape asymmetry and wall curvature.

Adam Wysocki, Jens Elgeti, and Gerhard Gompper<sup>1</sup>

<sup>1</sup>*Theoretical Soft Matter and Biophysics, Institute of Complex Systems and Institute for Advanced Simulation, Forschungszentrum Jülich, 52425 Jülich, Germany*

(Dated: May 12, 2015)

The effect of shape asymmetry of microswimmers on their adsorption capacity at confining channel walls is studied by a simple dumbbell model. For a shape polarity of a forward-swimming cone, like the stroke-averaged shape of a sperm, extremely long wall retention times are found, caused by a non-vanishing component of the propulsion force pointing steadily into the wall, which grows exponentially with the self-propulsion velocity and the shape asymmetry. A direct duality relation between shape asymmetry and wall curvature is proposed and verified. Our results are relevant for the design microswimmer with controlled wall-adhesion properties. In addition, we confirm that pressure in active systems is strongly sensitive to the details of the particle-wall interactions.

PACS numbers: 82.70.Dd, 87.10.Mn, 47.63.Gd, 87.17.Jj

Boundaries dominate biological process on all scales. On the microscopic scale, motile organism may bump into various obstacles and boundaries, such as liquid-gas or liquid-liquid interfaces, elastic cell membranes or solid walls. A universal behavior is the accumulation of microswimmers at boundaries [1, 2]. Aside from physico-chemical effects [3], such as van der Waals forces, two main mechanisms have been suggested to explain the wall accumulation, hydrodynamic interactions (HI) [4, 5] and excluded-volume (or steric) forces [6, 7]. The importance of HI on accumulation is still a subject of debate. However, recent experiment in quasi-2D microfluidic channels indicate that surface scattering of sperm and *Chlamydomonas* at lateral boundaries is dominated by steric forces with multiple flagellar contacts [8, 9], in strong contrast to sperm confined in a 3D channel, where HI seems to dominate adhesion [10].

Most theoretical studies of simple model swimmers, both in bulk and in confinement, have considered so far cells with a symmetric body shape, in particular, rods [6, 7] or spherical particles [11, 12]. In reality, however, cells usually do not exhibit such high symmetry, and the stroke-averaged shape of sperm or *Chlamydomonas* rather resembles a forward or a backward swimming cone, respectively [8, 9, 13], see also Fig. 1(b,c). This raises the question how a broken for-aft symmetry of the particle shape alters the wall accumulation of cells.

In order to elucidate shape effects on effective adsorption, we neglect HI and study a generic model of an active Brownian dumbbell with unequal bead sizes, see Fig. 1(a). Our simulation results show that swimmers with a sperm-like (polar) shape exhibit huge wall trapping times due to a nonvanishing component of the propulsion force directed steadily toward the wall, thus resulting in a restricted rotational movement. The trapping times increase exponentially with the shape asymmetry  $\theta_0$  and the propulsion strength  $V$  and could, for realistic parameters of  $\theta_0$  and  $V$ , exceed trapping times due to near-field hydrodynamic forces [5, 14, 15]. In con-

trast, microswimmers with *Chlamydomonas*-like (antipolar) shape behave similarly to symmetric rod-like particles.

Both in a natural environment and in microfluidic devices [9, 16, 17], microswimmers usually do not swim in straight, but rather in curved or branching microchannels. Therefore, the influence of surface curvature on accumulation of microswimmers [14, 18–22] is of great interest. Based on the analysis of an asymmetric particle near a flat boundary, we predict a direct duality relation between the effect of shape asymmetry and surface curvature on accumulation. For example, a polar microswimmer close to a flat wall behaves similarly to an apolar particle near a concave surface (e.g. a cavity). This is of high relevance for the design microswimmers with controlled wall-adhesion properties.

We model the microswimmer as a self-propelled Brownian dumbbell. The dumbbell consists of two spheres with radii  $a_1$  and  $a_2$  connected by a rigid rod of length  $l$ , see Fig. 1(a). Its orientation is characterized by a unit vector  $\mathbf{e}$  directed along the axis from sphere 2 to sphere 1. The equation of motion for the swimmer's center (midpoint between the sphere centers) is then

$$\dot{\mathbf{r}} = V\mathbf{e} + \Xi^{-1}\mathbf{F}_w + \boldsymbol{\eta}, \quad (1)$$

where  $V$  is the bare propulsion velocity,  $\Xi$  is the translational friction tensor,  $\mathbf{F}_w$  is the steric force due to swimmer-wall interaction and  $\boldsymbol{\eta}$  is a random velocity. The particle is confined in a channel of height  $L$  along the  $z$ -direction. The sphere  $\alpha \in \{1, 2\}$  interacts with the walls via a screened Coulomb potential  $U_\alpha$  [23] with a large inverse screening length  $\kappa$  and thus resembles a hard-sphere. The total dumbbell-wall force is  $\mathbf{F}_w = \mathbf{F}_1 + \mathbf{F}_2$  with  $\mathbf{F}_\alpha = -\nabla_{\mathbf{r}_\alpha} U_\alpha$  where  $\mathbf{r}_\alpha$  is the position of sphere  $\alpha$ . The Gaussian white-noise velocity  $\boldsymbol{\eta}$  obeys  $\langle \boldsymbol{\eta}(t)\boldsymbol{\eta}(t') \rangle = 2k_B T \Xi^{-1} \delta(t - t')$ , where  $k_B T$  is the thermal energy scale and  $\Xi = \gamma_{\parallel} \mathbf{e}\mathbf{e} + \gamma_{\perp} (\mathbf{I} - \mathbf{e}\mathbf{e})$  is the translational friction tensor with the friction coefficients  $\gamma_{\parallel}$  and  $\gamma_{\perp}$  for motions parallel and perpendicular to  $\mathbf{e}$ , respec-

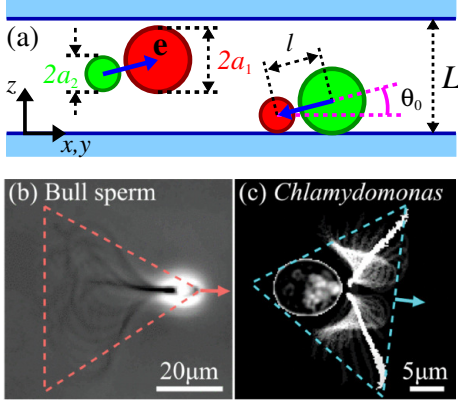


FIG. 1. (color online) (a) Sketch of the dumbbell model of asymmetric microswimmers in confinement. The swimmer propel along its instantaneous orientation  $\mathbf{e}$  with velocity  $V$  in a channel of height  $L$ . Left: a antipolar particle ( $\theta_0 > 0$ ); right: an polar particle ( $\theta_0 < 0$ ). (b,c) Experimental images. (b) Superimposed phase-contrast micrographs of swimming bull sperm; the cell mimics a forward-swimming cone (polar shape). (c) A *Chlamydomonas* alga, confined to quasi-2D motion, resembles a backward-swimming triangle (antipolar shape). Reprinted with permission from Ref. [13].

tively. The orientation evolves according to

$$\dot{\mathbf{e}} = (\mathbf{T}_w/\gamma_r + \boldsymbol{\xi}) \times \mathbf{e}, \quad (2)$$

where  $\boldsymbol{\xi}$  is a Gaussian white-noise vector with  $\langle \boldsymbol{\xi}(t)\boldsymbol{\xi}(t') \rangle = 2D_r\mathbf{I}\delta(t-t')$  and  $D_r = k_B T/\gamma_r$  is the rotational diffusion coefficient. The torque due to the wall interaction is  $\mathbf{T}_w = \mathbf{T}_1 + \mathbf{T}_2$  with  $\mathbf{T}_1 = (\mathbf{r}_1 - \mathbf{r}) \times \mathbf{F}_1 = l(\mathbf{e} \times \mathbf{F}_1)/2$  and  $\mathbf{T}_2 = -l(\mathbf{e} \times \mathbf{F}_2)/2$ . We solve Eqs. (1) and (2) numerically using standard methods [24].

Dimensionless numbers characterising the system are the Peclet number  $Pe = V/(lD_r)$ , which is the ratio of the swimming persistence length  $V/D_r$  to the rod length  $l$ , and the shape asymmetry parameter  $\sin(\theta_0) = (a_1 - a_2)/l$ , which is  $\sin(\theta_0) < 0$  for polar (sperm-like) and  $\sin(\theta_0) > 0$  for antipolar (*Chlamydomonas*-like) microswimmers. Wherever appropriate, we choose realistic parameters similar to that of *Escherichia coli* [25]. We increase swimming velocity up to  $Pe = 234$ ; for comparison, *Escherichia coli* achieve  $Pe \approx 120$  [5], while *Chlamydomonas* and bull sperm reach only  $Pe \approx 25 - 50$  due to the large active rotational diffusion [5, 26]. We consider only small asymmetry,  $|\sin(\theta_0)| \approx |\theta_0| \leq 0.125$ . Note that  $|\sin(\theta_0)| \approx 0.5$  for sperm and *Chlamydomonas* [13], see also Fig. 1(b,c). Furthermore, we apply a weak confinement with channel height  $L = 10l$ .

There are universal features in the behavior of an elongated microswimmer confined inside a channel. The swimmer performs a persistent random walk within the bulk region; when it encounters a wall, a torque, caused by steric interactions, leads to approximately parallel alignment with the wall; finally, the swimmer can escape

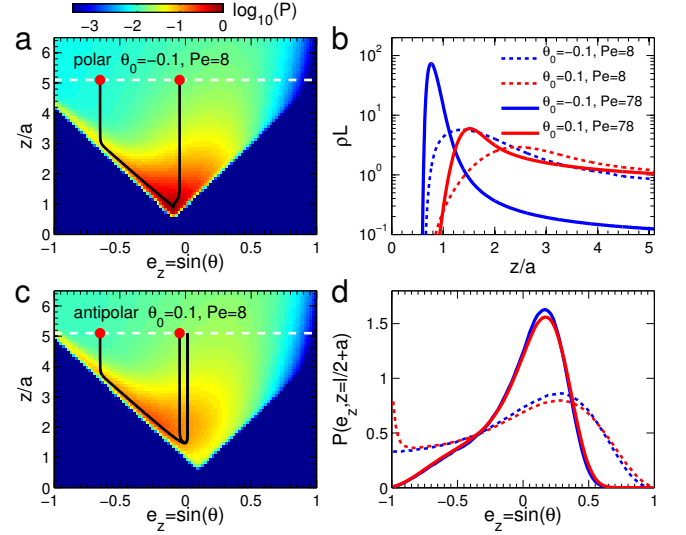


FIG. 2. (color online) (a,c) Logarithmically color-coded plots of the probability density function (PDF)  $P(e_z, z)$  at moderate activity  $Pe = 8$ . (a)  $P(e_z, z)$  for a polar ( $\theta_0 < 0$ ) and (c) an antipolar swimmer ( $\theta_0 > 0$ ). Deterministic trajectories are indicated by solid lines. A polar swimmer is highly localized at  $(e_z, z) = (\sin(\theta_0), a/2)$ . (b) The corresponding orientation-averaged PDF  $\rho(z) = \int_{-1}^1 P(e_z, z) de_z$ . (d) PDF of the orientation  $P(e_z, z \approx \delta)$  at the threshold of steric interactions ( $\delta = l/2 + a$ ), see dashed line in (a,c). Swimmers leave the wall region increasingly parallel with increasing  $Pe$ .

from the boundary when its orientation, as a result of rotational diffusion, points slightly away from the boundary [6, 7]. Generally, swimmers are increasingly localized near the wall with increasing activity, as can be seen from the density profile  $\rho(z)$  in Fig. 2(b). Shape asymmetry changes the behavior dramatically. Polar swimmers are much more strongly adsorbed as their antipolar counterpart, see Fig. 2(b). Moreover, polar particles point persistently toward the wall at an angle prescribed by the body shape, see high probability density at  $(e_z, z) = (\sin(\theta_0), a/2)$  in Fig. 2(a) and compare to the probability density function  $P(e_z, z)$  of a antipolar swimmer in Fig. 2(c). A high probability density near the boundary is tantamount to a large wall retention time. As can be seen in Fig. 3 and will be discussed in more detail below, the retention time of the particles indeed increases very rapidly with increasing activity and shape polarity.

In order to understand the giant wall accumulation of polar microswimmers, and in particular the huge trapping times, we examine Eqs. (1) and (2) with the focus on the two relevant variables, the coordinate along the surface normal  $z$  and the orientation angle  $\theta$ , see Fig. 1, which implies

$$\dot{z} = V \sin(\theta) + F_w/\gamma + \eta, \quad (3)$$

$$\dot{\theta} = -D_r \tan(\theta) + T_w/\gamma_r + \xi. \quad (4)$$

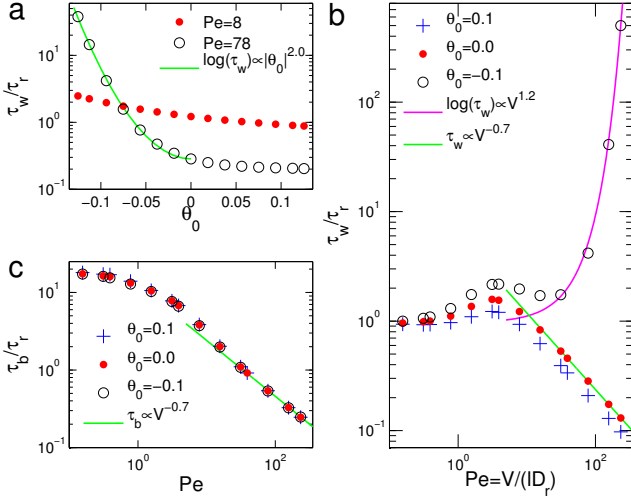


FIG. 3. (color online) (a) Mean time  $\tau_w$  a swimmer remains within the wall region ( $z \in [0, \delta]$  or  $z \in [L - \delta, L]$ ) as function of the shape asymmetry  $\theta_0$ ; time is normalized by  $\tau_r = 1/(2D_r)$ . (b)  $\tau_w$  versus  $Pe$ . For polar swimmers  $\tau_w$  grows exponentially with  $V$ , while for apolar and antipolar swimmers  $\tau_w \propto V^{-0.7}$ . (c) Mean time  $\tau_b$  a swimmer remains within the bulk region ( $z \in [\delta, L - \delta]$ ) versus  $Pe$ .  $\tau_b$  is independent of  $\theta_0$  and  $\tau_b \propto V^{-0.7}$  for  $Pe \gg L/l = 10$ .

The first term on the RHS of Eq. (4) is peculiar for rotational diffusion in 3D [15, 27] and can be neglected for  $Pe \gg 1$ . The noise obeys  $\langle \eta(t)\eta(t') \rangle = 2D\delta(t-t')$  with  $D = k_B T/\gamma = (D_{\parallel} + 2D_{\perp})/3$  and  $\langle \xi(t)\xi(t') \rangle = 2D_r\delta(t-t')$ . We linearize Eqs. (3) and (4) around the stable point  $(z^*, \theta^*) = (a/2, \theta_0)$  of a fully absorbed particle, and define small perturbation as  $(\delta z, \delta \theta) = (z - z^*, \theta - \theta^*)$ . The equations of motion then reduce to an Ornstein-Uhlenbeck process,

$$\frac{d}{dt} \begin{pmatrix} \delta z \\ \delta \theta \end{pmatrix} \approx \begin{pmatrix} \kappa V \theta_0 & V \\ 0 & \frac{\kappa l^2 \gamma V \theta_0}{4\gamma_r} \end{pmatrix} \begin{pmatrix} \delta z \\ \delta \theta \end{pmatrix} + \begin{pmatrix} \eta \\ \xi \end{pmatrix}, \quad (5)$$

where we assume small  $\theta_0$ . Our aim is to estimate the mean escape time  $\tau_e$ , i.e., the mean time to reach an orientation parallel to the wall,  $(z, \theta) = (a/2, 0)$ , from the stable position  $(z, \theta) = (z^*, \theta^*)$  by rotational diffusion. In order to do so, we reduce the complexity of the problem further by neglecting the motion normal to the surface,

$$\dot{\delta \theta} = -\frac{dU}{d\delta \theta} + \xi, \quad U = \frac{k}{2} \delta \theta^2. \quad (6)$$

Here,  $U$  is an effective harmonic potential for the orientation angle with spring constant  $k = -\kappa l^2 \gamma V \theta_0 / (4\gamma_r)$ .

The escape problem, Eq. (6), is related to a first passage problem. An exact expression of the mean first-passage time from any point along any potential to any other point exists [28]; however, due to the complexity of this expression, an extraction of the leading contributions seems unfeasible. A low-noise approximation is the

Kramers rate theory of crossing a smooth potential barrier [15, 28]; here, we use a heuristic expression for the mean escape time over a barrier  $\Delta U = U(\delta \theta_e) = U(-\theta_0)$ , which captures the low- and the high-noise limits [5],

$$\tau_e \approx \frac{\delta \theta_e^2}{D_r} \exp\left(\frac{\Delta U}{D_r}\right) = \frac{\theta_0^2}{D_r} \exp\left(-\frac{\kappa l^2}{8D} V \theta_0^3\right). \quad (7)$$

Note that  $\theta_0 < 0$  ( $\theta_0 > 0$ ) for polar (antipolar) particles.

In the simulations, we measure the mean trapping time  $\tau_w$  as the time during which the swimmer remains within the wall region (range of steric interactions:  $z \in [0, \delta]$  or  $z \in [L - \delta, L]$  with  $\delta = l/2 + a$ ). In case of polar swimmers, this trapping time is an estimate of  $\tau_e$ . As can be seen in Fig. 3, we do indeed observe exponential dependencies of  $\tau_w$  in the low-noise regime, with  $\log(\tau_w) \propto \theta_0^2$  in Fig. 3(a,b) and  $\log(\tau_w) \propto V$  in Fig. 3(c). The dependence of  $\tau_w$  on  $V$  is nicely consistent with Eq. (7); however, we observe  $\log(\tau_w) \propto \theta_0^2$  instead of  $\log(\tau_e) \propto \theta_0^3$ , as predicted by Eq. (7). Considering the various approximations in the derivation of Eq. (7), like the harmonic form of  $U(\delta \theta)$  and the dimension reduction, it is not surprising that we do not obtain a perfect agreement. In particular, the parabolic description of  $U$  breaks down with increasing  $\delta \theta$ ; moreover,  $U$  is a function of  $\delta z$  and should soften with increasing  $\delta z$ .

In case of apolar and antipolar swimmers, which do not point persistently toward the wall, the above treatment does not apply. Instead,  $\tau_w$  can be deduced from an analogy to a semi-flexible polymer adsorbed on a wall [6, 7], which predicts a scaling behavior  $\tau_w \propto V^{-2/3}$ , see Fig. 3(c). This process contributes also to  $\tau_w$  of polar particles, but it becomes negligible as compared to the escape time over the effective potential barrier  $\Delta U$  for large polarity and  $Pe \gg 1$ .

The mean time  $\tau_b$  a swimmer remains within the bulk region (outside the range of steric interactions) is independent of  $\theta_0$ . As can be seen from Fig. 2(d), particles leave the wall region increasingly parallel with increasing  $Pe$ . In agreement with the semi-flexible polymer analogy [6], we observe  $\langle \theta \rangle \propto V^{-1/3}$  at  $z \approx \delta$  in the ballistic regime. Thus, with  $\tau_b \propto L/(V \sin \langle \theta \rangle)$  we obtain  $\tau_b \propto L/V^{2/3}$  consistently with simulations, see Fig. 3(d).

With this knowledge, it is easy to interpret a global measure of the density distribution, the surface excess (or adsorption)  $\Gamma = \int_0^L [\rho(z) - \rho_b] dz$ , where  $\rho_b$  is the bulk density. For a passive hard dumbbell,  $\Gamma = -\delta/(L - \delta) < 0$ , while for fully absorbed particles it is  $\Gamma = 1$ . A rough estimate of  $\Gamma$  is

$$\Gamma \approx 2 \int_0^\delta \rho(z) dz - 2\rho_b \delta \approx \frac{2\tau_w - \tau_b 2\delta/(L - 2\delta)}{2\tau_w + \tau_b}. \quad (8)$$

Using the scaling of  $\tau_w$  and  $\tau_b$ , see Fig. 3, we obtain low- and high- $Pe$  limits, which are consistent with the simulation results, as indicated in Fig. 4(a).

The problem of a microswimmer with shape asymmetry moving near a planar wall bears a strong resemblance

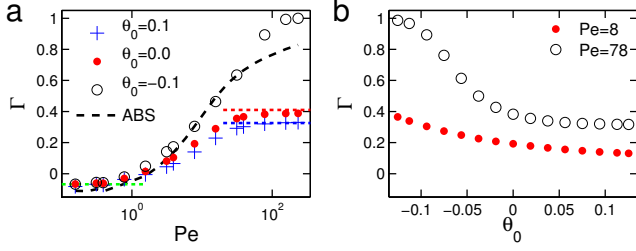


FIG. 4. (color online) (a) Adsorption  $\Gamma$  versus activity  $Pe$  for antipolar ( $\theta_0 > 0$ ), apolar ( $\theta_0 = 0$ ) and polar swimmer ( $\theta_0 < 0$ ). Asymptotic estimates of  $\Gamma$  are indicated by dashed lines.  $\Gamma$  of active Brownian spheres (ABS) is shown for comparison. Note that polar swimmers are completely absorbed ( $\Gamma = 1$ ) above a critical  $Pe$ , by contrast, apolar and antipolar swimmers are always partially absorbed. (b)  $\Gamma$  as function of the asymmetry  $\theta_0$  at various  $Pe$ .

with a swimmer moving near a curved wall, see Fig. 5. Let us consider first a apolar swimmer in spherical confinement of radius  $R$ , see Fig. 5(a). In this case, as in the case of a polar microswimmer at a planar wall, the velocity vector in the stable conformation forms an angle with the tangent plane to the wall at the front bead. Thus, in both cases, the microswimmer points toward the wall and thus should have very long retention times. Secondly, the force of a polar microswimmer towards the wall can be partially or fully compensated by a convex wall, i.e., for a microswimmer moving at the outer surface of a sphere of radius  $R$ , see Fig. 5(b). In the case of a full compensation, we predict the same accumulation behavior as for an apolar particle at a planar wall. Note that an apolar microswimmer would strongly scatter at convex wall. Thus, shape polarity provides the possibility for microswimmers to move along curved surfaces!

Hence, it is obvious to define a generalized asymmetry, considering shape asymmetry and wall curvature at once, as  $\Theta_0 \equiv \theta_0^s + \theta_0^w = (a_1 - a_2)/l + kl/(2R)$  for  $R \gg l \gg |a_1 - a_2|$ , where  $k = +1$  for convex and  $k = -1$  for concave boundaries. This allows a unified description of asymmetric microswimmers near curved walls, where  $\Theta_0 < 0$  ( $\Theta_0 > 0$ ) implies an exponential grow (algebraic decay) of  $\tau_w$  with  $V$ .

We have performed various test in order to verify the equivalence of shape asymmetry and surface curvature [29]. First, we analyse the behavior of an apolar microswimmer ( $\theta_0^s = 0$ ) close to a surface with a curvature ranging from that of a convex to a concave wall. The wall retention times  $\tau_w$  as a function of the generalized asymmetry  $\Theta_0 \equiv \theta_0^s + \theta_0^w$  and  $Pe$  are shown in Fig. 6(a,b). The results closely resemble the corresponding dependencies of a asymmetric swimmer near a flat wall in Fig. 3(a,b). However,  $\tau_w \propto V^{-1}$  for  $\theta_0^w > 0$  in contrast to  $\tau_w \propto V^{-0.7}$  for  $\theta_0^w = 0$ ; the  $\tau_w \propto V^{-1}$  behavior reflects a simple ballistic escape from convex walls. Further, we have tested whether shape polarity can be compensated by

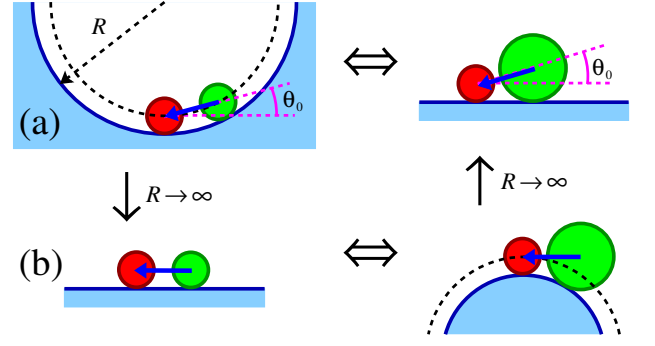


FIG. 5. (color online) (a) An apolar swimmer confined within a spherical cavity of radius  $R$  is equivalent to a polar swimmer close to a flat wall provided that the angle  $\theta_0 \approx -l/(2R)$ , between the propulsion force of the apolar swimmer and the tangent plane of the cavity at the front bead, equals the asymmetry  $\theta_0 \approx (a_1 - a_2)/l$  of the polar particle. (b) A polar particle near a convex boundary behaves like an apolar swimmer close to a flat wall if  $(a_1 - a_2)/l \approx -l/(2R)$ .

a negative curvature of the wall. We simulate a polar swimmer with fixed  $\theta_0^s = -0.09$  close to the surface of a sphere at different radii  $R$ , i.e., at different wall polarities  $\theta_0^{wall} = l/(2R)$ . The results for  $\tau_w$  as a function of  $\Theta_0$  and  $Pe$  are shown in Fig. 6(c). Again the similarity with the results in Fig. 3(b) is striking. Hence, a symmetric rod near a planar wall is equivalent to a polar swimmer near a convex boundary provided that shape and wall polarity cancel, i.e.,  $\Theta_0 \approx 0 \Rightarrow (a_1 - a_2)/l \approx -l/(2R)$ .

Finally, we want to briefly discuss the the wall pressure in active systems. There are several attempts to construct an equation of state for active fluids [30–32]. However, this idea has been questioned, because the pressure  $p$ , measured as the force exerted on the boundary per wall area, should strongly depends on the details of the swimmer-wall interaction [33], in contrast to thermal equilibrium. Our results support the latter claim. We observe that, in contrast to active Brownian spheres where  $p \propto V$  in the strong confinement limit ( $Pe \gg L/l$ ) [30, 34],  $p \propto V^{1.35}$  for polar swimmers, and  $p \propto V^{0.42}$  for symmetric rods and antipolar particles, see Fig. 7. The difference between a spherical and a rod-like particle is that the latter exert a significant force only during the arrival at the wall, and align immediately parallel with the boundary due to the steric torque  $T_w(e_z, z)$ .

In summary, we have shown that a small shape polarity of microswimmers leads to extremely long wall-trapping times. The exponential dependence of  $\tau_w$  on  $V$  and  $\theta_0$  is responsible for a nearly complete adsorption of polar particles, in contrast to symmetric rods or antipolar particles. The pressure  $p$  in active system is sensitive to the details of the swimmer-wall interaction [33], in particular the variation of the asymmetry from antipolar to polar change the grow of  $p$  with  $V$  from sublinear to superlinear.

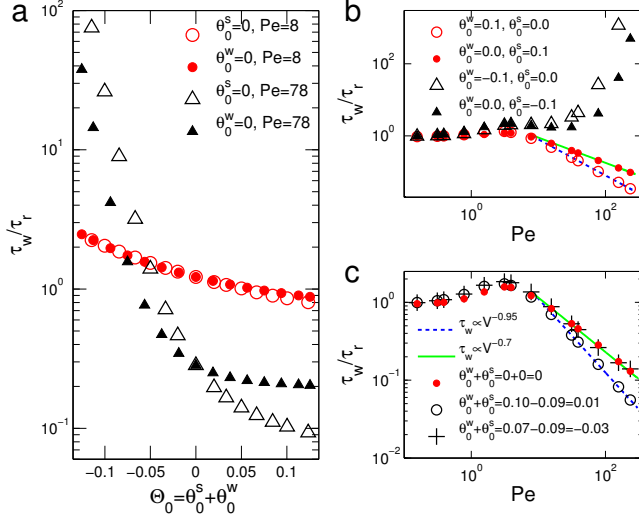


FIG. 6. (color online) Equivalence of body shape and wall curvature.  $\theta_0^w < 0$  corresponds to a motion within a spherical cavity and  $\theta_0^w > 0$  means swimming close to the outer surface of a sphere.  $\tau_w$  is shown as a function of the generalized asymmetry  $\Theta_0 \equiv \theta_0^s + \theta_0^w$  and  $Pe$ . (a,b) An apolar swimmer ( $\theta_0^s = 0$ ) near curved boundaries ( $\theta_0^w \neq 0$ ); the situation is illustrated in Fig. 5(a). Filled symbols indicate  $\tau_w$  of an asymmetric swimmer ( $\theta_0^s \neq 0$ ) near a flat wall ( $\theta_0^w = 0$ ). (c) A polar swimmer ( $\theta_0^s = -0.09$ ) near a convex wall ( $\theta_0^w > 0$ ); the situation is illustrated in Fig. 5(b). In (b) and (c) the same power-law decays are indicated by lines.

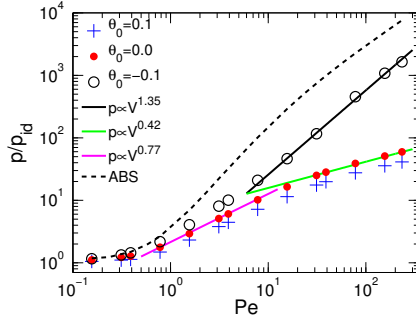


FIG. 7. (color online) Active pressure  $p$  as a function of  $Pe$  normalized with the ideal gas pressure  $p_{id}$ . At large activity pressure grows superlinear for polar swimmers and sublinear for symmetric rods and antipolar particles.  $p$  of active Brownian spheres (ABS) is shown for comparison [30, 34].

We have neglected HI in our analysis to elucidate the effects of swimmer shape on wall adsorption. However, it is worthwhile to briefly speculate on the interplay of both effects. We restrict our discussion to pushers, i.e., to micro-organisms and self-propelled particles that generate thrust behind the body, such as sperm or bacteria. The retention time due to HI,  $\tau_e^{HI}$ , corresponds to the time to reach an angle  $\theta_e^{HI} > 0$  starting from parallel, where self-propulsion outweighs hydrodynamic attraction [5].  $\tau_e^{HI}$  has been predicted to follow an Arrhenius-

Kramer-like behavior [5, 15]. For a polar pusher, the effective potential for the orientation angle now contains two barriers at  $\theta = 0$  (due to shape) and  $\theta = \theta_e^{HI}$  (due to HI). Thus, a naive expectation would be that the resulting retention time is a sum of the retention times due to shape and HI [35]. However, we expect a synergistic effect, because hydrodynamic interaction will both additionally attract the swimmer towards the wall and further restrict rotational movement, which increases the effective barrier height. In contrast, for antipolar pushers, hydrodynamic attraction will favor a configuration with orientation pointing away from the wall, and hence can be expected to shorten the way to the potential barrier due to HI at  $\theta_e^{HI} > 0$ , thereby ultimately decreasing HI-induced wall adhesion.

Furthermore, we have shown that wall curvature can compensate the effect of shape asymmetry, i.e., asymmetry and curvature are two sides of the same coin. Thus, the combination of both effects can be used in order to design artificial microswimmers or microfluidic devices for particular tasks. For example, microswimmers could be designed which move along surfaces within a porous medium [20, 36], while corrugated microfluidic channels can be constructed to reduce wall accumulation [9, 22].

We thank J. Hu, G. Schütz, A. Varghese, and R. G. Winkler for helpful discussions. We gratefully acknowledge support by the DFG within the priority program SPP 1726 “Microswimmers”.

- 
- [1] E. Lauga and T. R. Powers, Reports on Progress in Physics **72**, 096601 (2009).
  - [2] J. Elgeti, R. G. Winkler, and G. Gompper, Rep. Prog. Phys. **78**, 056601 (2015).
  - [3] H. H. Tuson and D. B. Weibel, Soft Matter **9**, 4368 (2013).
  - [4] A. P. Berke, L. Turner, H. C. Berg, and E. Lauga, Phys. Rev. Lett. **101**, 038102 (2008).
  - [5] K. Drescher, J. Dunkel, L. H. Cisneros, S. Ganguly, and R. E. Goldstein, Proc. Natl. Acad. Sci. USA **108**, 10940 (2011).
  - [6] J. Elgeti and G. Gompper, EPL **85**, 38002 (2009).
  - [7] G. Li and J. X. Tang, Phys. Rev. Lett. **103**, 078101 (2009).
  - [8] V. Kantsler, J. Dunkel, M. Polin, and R. E. Goldstein, Proc. Natl. Acad. Sci. USA **110**, 1187 (2013).
  - [9] P. Denissenko, V. Kantsler, D. J. Smith, and J. Kirkman-Brown, Proc. Natl. Acad. Sci. USA **109**, 8007 (2012).
  - [10] J. Elgeti, U. B. Kaupp, and G. Gompper, Biophys. J. **99**, 1018 (2010).
  - [11] J. Elgeti and G. Gompper, EPL **101**, 48003 (2013).
  - [12] C. F. Lee, New J. Phys. **15**, 055007 (2013).
  - [13] H. H. Wensink, V. Kantsler, R. E. Goldstein, and J. Dunkel, Phys. Rev. E **89**, 010302 (2014).
  - [14] S. E. Spagnolie, G. R. Moreno-Flores, D. Bartolo, and E. Lauga, Soft Matter **11**, 3396 (2015).
  - [15] K. Schaar, A. Zöttl, and H. Stark, arXiv:1412.6435



- (2014).
- [16] B. Kaehr and J. B. Shear, *Lab Chip* **9**, 2632 (2009).
- [17] H. Wioland, F. G. Woodhouse, J. Dunkel, J. O. Kessler, and R. E. Goldstein, *Phys. Rev. Lett.* **110**, 268102 (2013).
- [18] S. van Teeffelen, U. Zimmermann, and H. Löwen, *Soft Matter* **5**, 4510 (2009).
- [19] Y. Fily, A. Baskaran, and M. F. Hagan, *Soft Matter* **10**, 5609 (2014).
- [20] D. Takagi, J. Palacci, A. B. Braunschweig, M. J. Shelley, and J. Zhang, *Soft Matter* **10**, 1784 (2014).
- [21] I. D. Vladescu, E. J. Marsden, J. Schwarz-Linek, V. A. Martinez, J. Arlt, A. N. Morozov, D. Marenduzzo, M. E. Cates, and W. C. K. Poon, *Phys. Rev. Lett.* **113**, 268101 (2014).
- [22] H. A. Guidobaldi, Y. Jeyaram, C. A. Condat, M. Oviedo, I. Berdakin, V. V. Moshchalkov, L. C. Giojalas, A. V. Silhanek, and V. I. Marconi, *Biomechanics* **9**, 024122 (2015).
- [23] The sphere  $\alpha \in \{1, 2\}$  interacts with the lower wall via
- $$\frac{U_\alpha}{k_B T} = 10 \frac{\exp[-\kappa(z_\alpha - a_\alpha)]}{\kappa(z_\alpha - a_\alpha)}, \quad (9)$$
- and equivalently with the upper wall, where  $z_\alpha = \mathbf{r}_\alpha \hat{\mathbf{z}}$  is the  $z$ -coordinate of sphere  $\alpha$ . Strong screening is achieved by using  $\kappa a = 10$ .
- [24] H. Löwen, *Phys. Rev. E* **50**, 1232 (1994).
- [25] Using realistic parameters for *Escherichia coli* [5], we set length scales to  $l = 8 \mu\text{m}$  and  $a = a_1 + a_2 = 1 \mu\text{m}$ , diffusion constants to  $D_\parallel = 0.149 \mu\text{m}^2/\text{s}$ ,  $D_\perp = 0.135 \mu\text{m}^2/\text{s}$ , and  $D_r = 0.032 \text{s}^{-1}$ . We vary  $Pe$  by changing  $V$  up to  $60 \mu\text{ms}^{-1}$ .
- [26] C.-K. Tung, F. Ardon, A. Roy, D. L. Koch, S. S. Suarez, and M. Wu, *Phys. Rev. Lett.* **114**, 108102 (2015).
- [27] M. Raible and A. Engel, *Appl. Organomet. Chem.* **18**, 536 (2004).
- [28] P. Hänggi, P. Talkner, and M. Borkovec, *Rev. Mod. Phys.* **62**, 251 (1990).
- [29] For the simulations of a microswimmer near a convex wall, we fill the space between two spheres of the dumbbell with additional spherical segments with diameters interpolating linearly between the front and back spheres, similar to Ref. [13].
- [30] X. Yang, M. L. Manning, and M. C. Marchetti, *Soft Matter* **10**, 6477 (2014).
- [31] S. C. Takatori, W. Yan, and J. F. Brady, *Phys. Rev. Lett.* **113**, 028103 (2014).
- [32] F. Ginot, I. Theurkauff, D. Levis, C. Ybert, L. Bocquet, L. Berthier, and C. Cottin-Bizonne, *Phys. Rev. X* **5**, 011004 (2015).
- [33] A. Solon, Y. Fily, A. Baskaran, M. Cates, Y. Kafri, M. Kardar, and J. Tailleur, *arXiv:1412.3952* (2014).
- [34] S. A. Mallory, A. Šarić, C. Valeriani, and A. Cacciuto, *Phys. Rev. E* **89**, 052303 (2014).
- [35] H. Risken, *Fokker-Planck Equation* (Springer, 1984).
- [36] A. T. Brown, I. D. Vladescu, A. Dawson, T. Vissers, J. Schwarz-Linek, J. S. Lintuvuori, and W. C. Poon, *arXiv:1411.6847* (2014).